Phase transition from Au–Te surface alloy towards tellurene-like monolayer

Meryem Bouaziz, Wei Zhang, Yongfeng Tong, Hamid Oughaddou, Hanna Enriquez, Rym Mlika, Hafsa Korri-Youssoufi, Zhesheng Chen, Heqi Xiong, Yingchun Cheng, et al.

Phase Transition from Au_2Te Surface Alloy towards Tellurene-type Monolayer

Meryem Bouaziz[1,2,3], Wei Zhang[4], Yongfeng Tong[1], Hamid Oughaddou [4,5], Hanna Enriquez [4], Rym Mlika[2], Hafsa Korri-Youssoufi[3], Zhesheng Chen[1], Heqi Xiong[6], Yingchun Cheng[6]* and Azzedine Bendounan[1]*

[1]*Synchrotron SOLEIL, L'Orme des Merisiers, Saint-Aubin – BP 48, F-91192, Gif-sur-Yvette Cedex, France*
[2]*Laboratoire des interfaces et matériaux avancés, Université de Monastir, 5019 Monastir, Tunisie*
[3]*Institut de Chimie Moléculaire et des Matériaux d'Orsay, Université Paris-Sud, 91400 Orsay Cedex, France*
[4]*Institut des Sciences Moléculaires d'Orsay, Université Paris-Sud, 91405 Orsay Cedex, France*
[5]*Département de Physique, Université de Cergy-Pontoise, Cergy-Pontoise Cedex 95031, France*
[6]*Key Laboratory of Flexible Electronics & Institute of Advanced Materials, Jiangsu National Synergetic Innovation Center for Advanced Materials, Nanjing Tech University, 30 South Puzhu Road, Nanjing 211816, People's Republic of China*

* Corresponding authors: azzedine.bendounan@synchrotron-soleil.fr; Tel.: +33-169-35-9799
iamyccheng@njtech.edu.cn

Abstract

We discuss here the structural and electronic properties of Au(111) surface after being exposed to high temperature vapor deposition of Tellurium (Te) in ultrahigh vacuum. The scenarios entailing the formation of $AuTe_2$ metal dichalcogenide or rather Au_2Te alloy monolayer or even *tellurene* single layer deserved to be addressed. In this purpose, low energy electron diffraction (LEED) supported by scanning tunneling microscopy (STM) shows the existence of several surface reconstructions depending on the Te film thickness in the sub-monolayer regime. We observed that the well-known spin-split Shockley state of the Au(111) surface survives the Te deposition and is even shifted to higher binding energy, suggesting a charge transfer at the interface. For a coverage of 0.33ML of Te, new dispersive bands are observed by angle-resolved photoemission (ARPES), which arise from a strong hybridization between the electronic states of Te and Au. With a substantially low intensity and a back-folding at the boundaries of the reduced surface Brillouin zone, these electronic bands represent a proof of the existence of a naturel 2D electron gas, strongly disturbed by the surface reconstruction. It is therefore possible that an Au_2Te alloy forms on the surface. By increasing the coverage to 0.5ML, a rich, thickness-dependent transition develops from the surface alloy to tellurene-like structure and completely excludes the growth of $AuTe_2$ monolayer on the surface. Both the surface alloy and the tellurene-type monolayer have a semiconductor character with a gap in the occupied states of 0.65 eV.

TOC

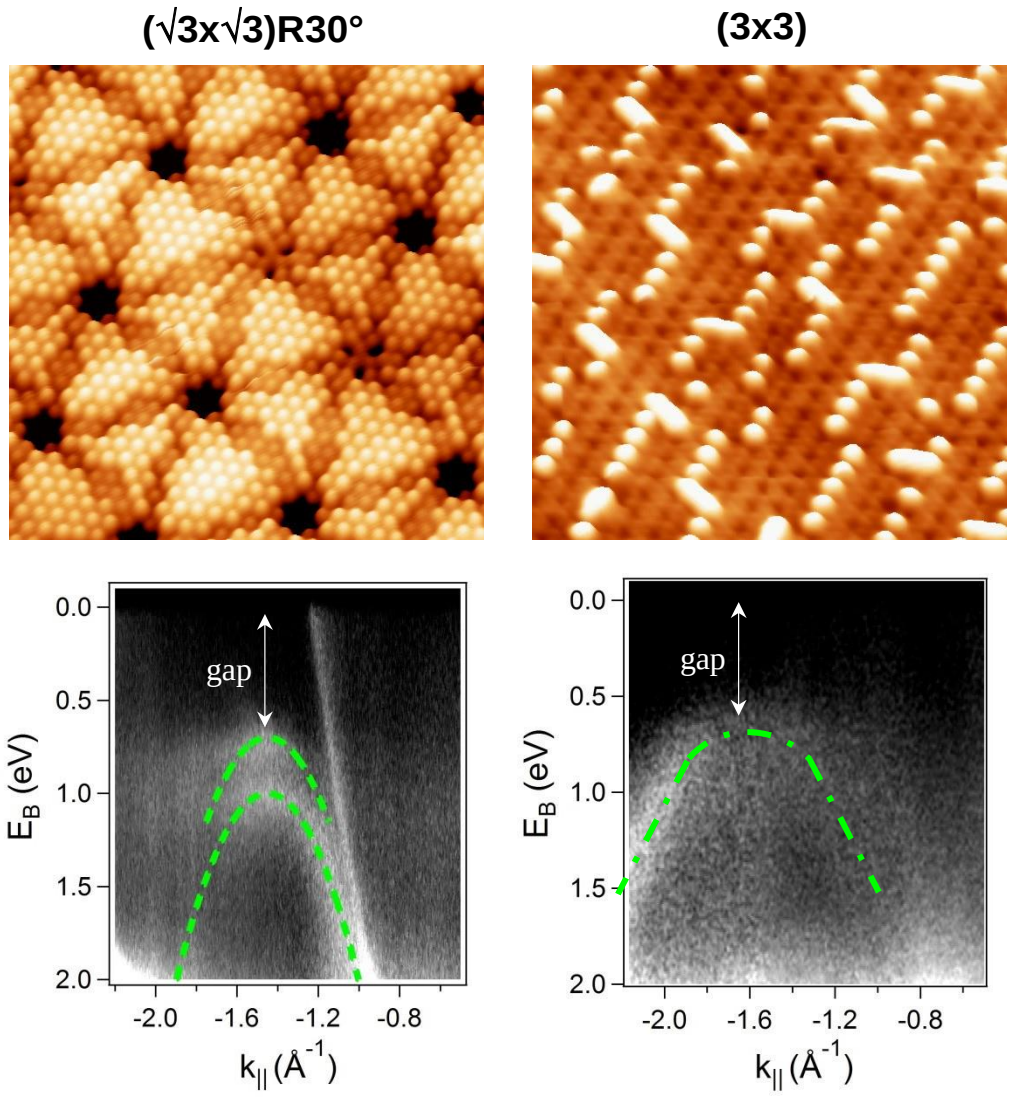

1. Introduction

In the recent years, two dimensional (2D) materials have attracted enormous scientific and technological interests. In particular, the transition metal dichalcogenides (TMDs) in the monolayer or multilayer regimes have received increasing and impressive attention due to the remarkable success in combining their unique optoelectronic properties with their reduced dimensions at the nanometer scale[1]. In fact, their intrinsic band gap is thickness dependent, thus makes them as a promising alternative to the most studied 2D materials, i.e. graphene, which lacks an intrinsic band gap. For example, MoS_2 monolayer exhibits a direct energy gap of 1.8 eV and pronounced photoluminescence[2,3], while bulky MoS_2 has a trivial photo-response and an indirect band-gap. In addition, size reduction of the TMDs systems can induce highly sought-after exotic properties, such as superconductivity[4,5], charge density waves[6], Quantum spin Hall effect[7], and valley-spin splitting[8,9].

Tellurium (Te)-based TMDs constitute ideal model systems for fundamental and technological researches. Being the heaviest non-radioactive element of the chalcogen group, Te is characterized by high air stability, strong spin-orbit coupling and a p-type semiconductor nature, which are valuable parameters for modern high-level technological applications. Te is also a monotonically tuned bandgap semiconductor with decreasing thickness from 0.33eV in a Te solid crystal to 1.0eV in the 2D monolayer system. On the other hand, noble metal surfaces, especially Au(111), can provide a platform for hosting an epitaxial TMD layer or binary surface alloy, both of which may accommodate fascinating 2D electron gas. Indeed, the in-situ deposition of Te on metallic surfaces (M) does not necessarily form TMD monolayers of MTe_2 composition, but can also generate a monolayer of surface alloy as M_2Te. In recent study, we have identified Cu_2Te alloy monolayer as an interesting new 2D material[10], which was also confirmed by another group[11]. This behavior seems to depend on the metal substrate itself because epitaxial growth of Se on Pt(111) leads to the formation of $PtSe_2$ having identical properties to MoS_2 sheets[12,13]. Also, it was shown that co-deposition of Te and Pt on 6H-SiC(0001) yields to the formation of $PtTe_2$ film[14]. For practical purpose, the monolayer of Te proved to be an ideal buffer layer to decouple blue phosphorus film from the Au substrate[15]. More interesting, it has been reported that Te doping boosts the transport performances and the stability to air of black phosphorus based Field Effect Transistors[16]. In the herein study, we characterized the atomic and electronic structures of low amount of Te (in the submonolayer regime) deposited by UHV-MBE on Au(111). One of the expected scenarios is the formation of one monolayer of $AuTe_2$. This composite called also *Calaverite,* is the most common gold

mineral and is the only compound in nature from which one can extract gold on an industrial scale. Moreover, it develops a superconductivity phenomenon when doped with Pt[17](Pd[18]) or submitted to high pressure[19]. To our limited knowledge, there is to date no evidence of an epitaxial or isolated monolayer of $AuTe_2$. The second scenario is the formation of an Au_2Te surface alloy, where Te atoms are embedded in the topmost Au layer, as has been effectively demonstrated for the other two noble metals Cu and Ag. A third scenario is also plausible, which consists of the emergence of the so-called "*tellurene*" monolayer floating on the Au(111) surface, as in the case of flat stanene on Cu(111)[20,21]. In fact, tellurene, an unaltered monolayer of Te with a honeycomb structure, has been successfully synthesized and employed in high-tech applications, due to its large on/off ratios, excellent ambient condition stability, and high carrier mobility[22-24].

Although the atomic structure of Te/Au(111) was the subject of long discussion[25-30], its electronic structure is still unexplored and no literature referring to the behavior of the valence electrons is reported up to day. After deposition of Te, the well-known $23x\sqrt{3}$ herringbone reconstruction is lifted, which suggests strong Te-Au interaction at the surface. Thereby, we present systematic investigation using complementary techniques to analyze the interplay between structural and electronic properties. Through LEED and STM, we have exanimated the crystal structure and atomic arrangement of the surface. To learn about the interaction inducing a chemical shift, XPS measurements were performed on the Au4f and Te4d core levels. The effect of the surface reconstruction depending on the Te coverage was systematically analyzed. Interestingly, by ARPES we have studied in detail the characteristics of the Shockley state, as well as new spectroscopic bands that result from hybridization between Te and Au electronic states. A structural phase transition depending on the Te coverage is observed and the formation of tellurene-type monolayer showing a honeycomb-like structure is suggested.

2. Experiment

Sample preparation: the Au(111) surface was prepared in-situ by standard procedure of multiple cycles consisting of Ar^+ sputtering followed by annealing at 500°C in ultra-high vacuum (UHV). The surface cleanliness was monitored by high-resolution XPS on the carbon and oxygen core levels, while the crystalline structure of the surface was characterized by LEED. For the present work, we have used a home-made Knudsen cell for the evaporation of Te in UHV. The evaporation rate was monitored by quartz microbalance and calibrated with respect to reference data from the literature[25]. We have also employed an alternative method based on chemical deposition that proved to give the same results and be successfully utilized for

elaboration of other systems[10,13]. It consists in immersion of the Au(111) substrate in 0.1 ML $NaTe_2$ solution for few minutes. The resulting surface is then well rinsed with Milli-Q water and dried under N_2 flow before reintroducing into the UHV analysis chamber for LEED, STM and XPS analysis.

Characterization: to carry out the high-resolution photoemission experiments we used the synchrotron radiation at TEMPO Beamline of Synchrotron SOLEIL, France. For probing the Au and Te core levels it was necessary to utilize photon energy of 260eV, which represents a compromise for obtaining reasonable photoionization cross section and high energy resolution (estimated of about 50meV). The ARPES measurements were made with photon energy of 60eV in excellent conditions of high energy and angle resolutions. The energy scale was also calibrated with the $Au4f_{7/2}$ on a clean Au(111) surface at the corresponding photon energy. The experimental binding energy calibration error for the reported core level binding energies (CLBE) is estimated to be of ±50 meV. LEED and Low temperature STM measurements were conducted on an Omicron STM station at ISMO-CNRS laboratory, Paris-Saclay University. The temperature reached 77K with liquid N_2 cooling during measurements. No further treatment of the STM images was applied.

3. Results description

3.1. LEED and STM investigations

First, we review here how the atomic structure of the Au(111) surface evolves after deposition of Te. Fig.1 displays large size STM topographies obtained on clean and covered Au(111) surface by Te sub-monolayer amounting to 0.33ML and 0.5ML, respectively. As expected, the pristine Au(111) surface shows the well-known herringbone reconstruction which originates from an uniaxial contraction of about 4.4% of the surface topmost layer with respect to the bulk, resulting in a reduction of the lateral Au-Au interatomic separation at the surface[31,32]. Thus, due to this constraint, the Au surface atoms occupy *fcc* or *hcp* sites of the underlying bulk lattice and 23 surface atoms occupy 22 substrate positions along the close-packed [1-10] direction[31]. The regions with high density of Au atoms appears as bright stripes in the STM image and correspond to the so-called domain walls or soliton walls which separate the wide *fcc* and narrow *hcp* regions[31]. We observe that this peculiar reconstruction of Au(111) is lifted when Te atoms are deposited on the surface. Such an effect is attributed to the reduction of the surface stress *via* charge redistribution induced by the Te electronegative adsorbates. Thus, this lifting of reconstruction is accompanied by the release of gold atoms from the herringbone structure. Note that when the adsorbate binds to the Au(111) surface by a simple van der Waals-like

interaction, the herringbone reconstruction remains imperturbable, as has been observed for organic molecular films[33,34] and also surprisingly after the deposition of Sn on Au(111), which induces a $SnAu_2$ alloy on the surface[35]. For the present system, even a slight variation in Te coverage causes a radical change of the atomic arrangement, as shown in Fig.1. Note however that the STM topographies display surfaces completely covered with very ordered superstructures at great distances. According to literature results, the formation of isolated and large islands of pure Te is excluded and, instead, the Te atoms are statistically distributed over the entire surface even at a very low coverage[26] and substitute Au atoms of the topmost surface layer when the thickness exceeds 0.24ML[25].

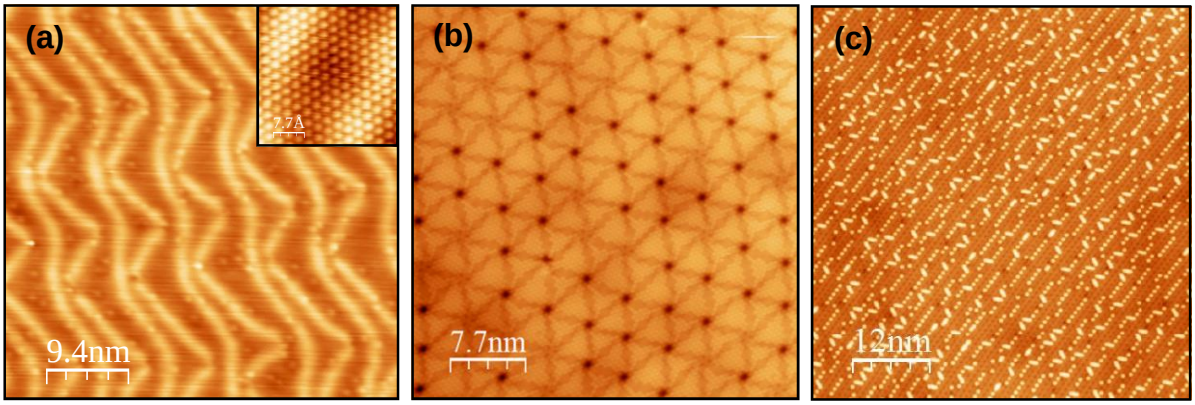

Fig.1: (a) Large-scale STM image of clean Au(111) surface, showing the herringbone reconstruction (U=-0.7V, I=1.0nA) and insert displays the associated image with atomic resolution. (b,c) Large-scale images measured on Au(111) covered by 0.33 ML and 0.5 ML of Te, respectively.

For Te coverage of about 1/3 ML, the surface exhibits a $(\sqrt{3}x\sqrt{3})R30°$ super-lattice, with Te atoms in the *hollow* site positions. Such a reconstruction has also been observed for Te/Cu(111)[10] and Te/Ag(111)[36], and for many other systems[37-39]. In addition, there is the co-existence of another reconstruction of a $(3\sqrt{21}x3\sqrt{21})R10°$ super-periodicity, as previously shown[25]. At coverage of ~ 0.5 ML, the morphology changes significantly and new reconstruction occurs at the surface, which consists of highly ordered honeycomb-like structure at large distance, as demonstrated in Fig.1c. Moreover, on-top of the reconstructed surface upper-layer, self-organization phenomenon of adatoms or clusters is observed. In fact, the adatoms occurring as bright dots in the STM image form well-defined and oriented atomic chain structures.

In the following, more detail is given on the atomic structure and the distribution of the Te atoms within the topmost surface layer. LEED patterns together with the corresponding atomically resolved STM images, as well as the profile line details are reported in Fig.2.

At Te coverage of about 0.25ML, it was shown that (√3x√3)R30° superstructure starts to develop on the surface[25]. In addition, it was demonstrated that a large scale reconstruction type (√111x√111)R4.7° is also present[25]. Here, we restrict ourselves to two characteristic Te thicknesses: 0.33 ML and 0.5ML.

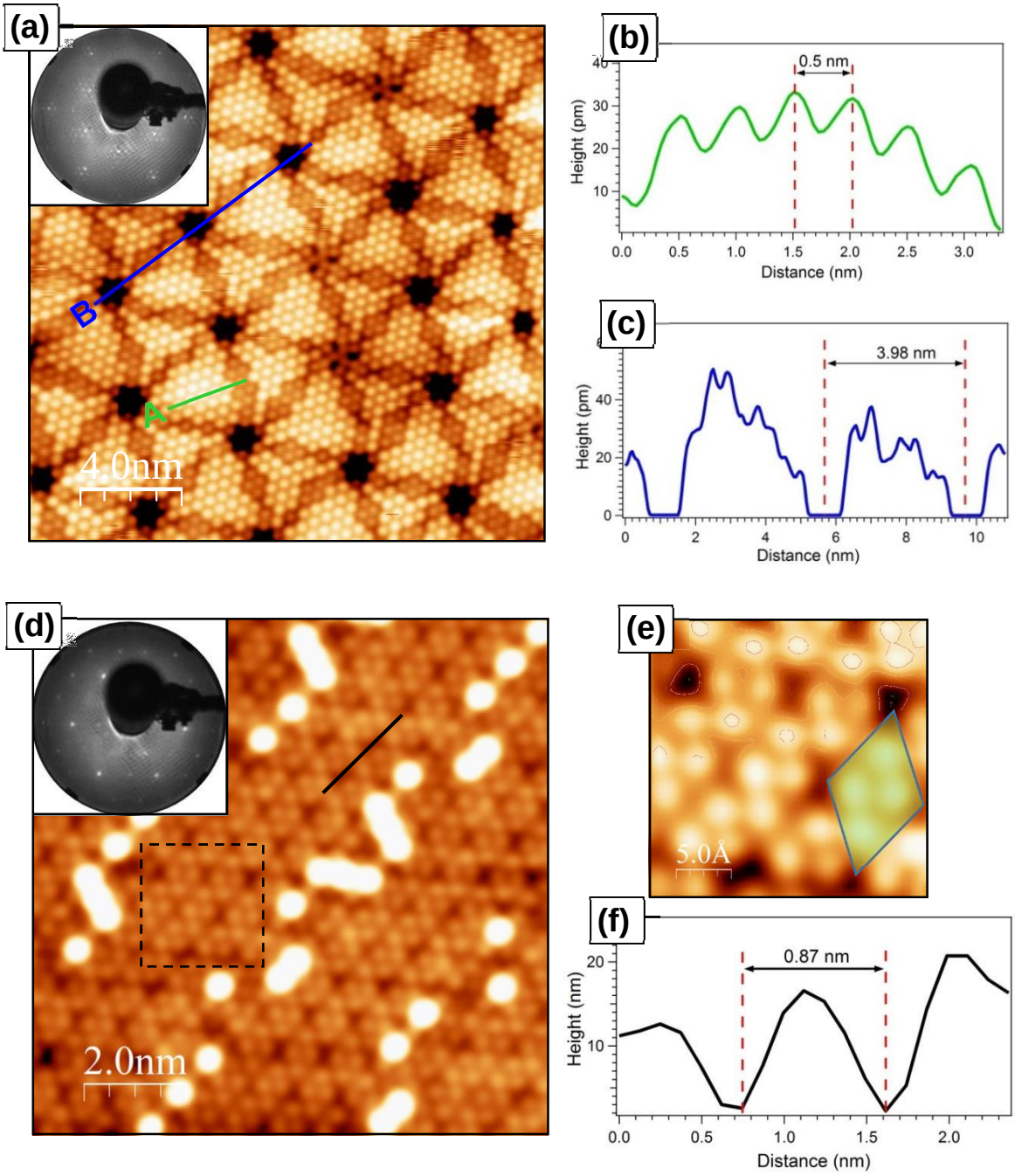

Fig.2: Quantitative analysis of STM images with atomic resolution obtained on Te/Au(111) system: (a) image at 0.33ML of Te, where the surface shows the coexistence of moiré and (√3x√3)R30° reconstructions, which are also highlighted in the LEED pattern given in the insert. (b,c) Profiles taken respectively along lines A and B indicated in image (a). (d) STM image at 0.5ML of Te displaying a honeycomb-like superstructure on which self-organization mechanism of Te atoms is observed. (e) Close STM inspection of the honeycomb-like network characterized by (3x3) super-lattice, as demonstrated by LEED (insert) and by the profile shown in (f) taken along line C in figure (d).

Indeed, by increasing the Te coverage to 0.33ML, the surface evolves sensively at the atomic scale. As shown in Fig.2a, the STM image reveals a highly structured surface and the LEED pattern (in inset) indicates the coexistence of two types of superstructure. The (√3x√3)R30° reconstruction is preserved whereas the 2D rhombus phase changes to another reconstruction with larger supercell (3√21x3√21)R10°. Thereby, the supercell size of √111 2D is converted to 3√21 by adding Te atoms. There is also a change in the orientation of the rhombus phase from 4.7° to 10°. From the STM image, we can destinguish a periodic flower-shaped pattern characterized by ordered arrows forming diamond-like patches that are abutted by two triangles. There are dark and bright patterned Te atoms, which are all sitting on (√3x√3)R30° superlattice with inter-distance of 0.5nm (Fig.2b). The distance between the centers of the flower feature is approximately 4nm, as obtained from the profile line shown in Fig.2c. This value is consistent with the moiré superstructure of (3√21x3√21)R10° periodicity. Because of the large radius of Te atoms, there is no sufficient space for them to always sit on the exact same 3-fold sites of Au(111). This leads to the formation of dark furrows along the edge of the diamond structure, where the Te atoms on each side are in different 3-fold sites and slightly further apart. On one side of a furrow, the atoms are on face-centered cubic (*fcc*) sites whereas the atoms on the other side are on hexagonal close-packed (*hcp*) sites.

When the Te coverage reaches 0.5 ML, one observes a honeycomb-like structure characterized by holes forming super-cell with hexagonal symmetry, as shown in Fig.2d,e. Careful examination of a line profile (Fig.2f) yields an average hole spacing (between two successful depletion regions) of approximately 8.7 Å, which corresponds to 3x the Au(111) lattice parameter. This is the signature of a (3x3) reconstruction, which is confirmed in the LEED pattern reported in the inset of Fig.2d and occurs in perfect accord with the literature[25]. Additionally, small clusters of Te adatoms nucleate on the holes of honeycomb-like structure and tend to align in quasi-1D chains following the symmetry direction of the honeycomb-like superstructure underneath. There are two types of adatom rows. On the one hand, relatively long rows composed of separate adatoms and, on the other hand, very dense and short rows. Indeed, the dominant distance between neighboring adatoms is 8.70 Å, while its value within the dense rows averages about 4.35 Å. The spacing between chains varies between 8.7 Å and 34.5 Å.

3.2. Photoemission analysis

Fig.3 shows the XPS spectra measured on Au(111) surface covered by 0.5ML of Te, recorded at normal and grazing emission angles, respectively. The spectra display an intense doublet due to electrons photo-emitted from the Au $4f_{7/2}$ (84eV) and $Au4f_{5/2}$ (87.6eV) core levels and very weak structures attributed to the Au5p levels. Deposition of Te film provokes the occurrence of spectroscopic features at binding energy of around 41 eV, which are assigned to the Te4d core levels. Note that the low intensity of the Te4d peaks compared to the Au4f is related to the effect of the photoionization cross section, which is significantly larger for Au4f than for Te4d at the selected photon energy (260eV)[40]. The spectral weight of the Te4d photoelectrons increases as we move from the normal to the grazing emission geometry, while the opposite effect is observed for Au4f. This means that the Te atoms are mostly on the surface of the sample and indicates the absence of any segregation process of Au atoms to the surface.

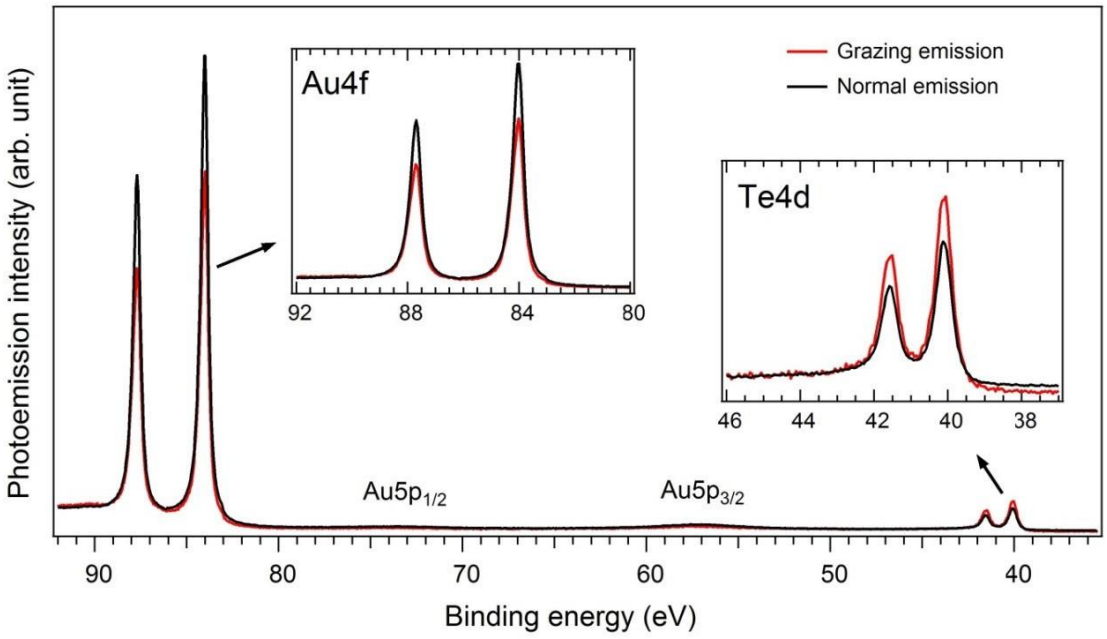

Fig.3: XPS spectra measured with hν=260 on Au(111) covered by 0.5ML of Te at normal and grazing emission geometries, respectively. Zooms are given on the Au4f and Te4d core levels.

Fig.4 illustrates a comparison between the Au4f spectra of the clean Au substrate and that after deposition of Te. The main component of the Au $4f_{7/2}$ peak at 84.0eV is associated with bulk Au (Au_B), whereas the shoulder at 83.66eV is associated with the reconstruction of the Au surface atoms (Au_S), since its intensity increases at the grazing emission geometry at which the surface contribution becomes high[41]. After substation of a Shirley background, the experimental spectrum was deconvoluted into two components Au_B and Au_S as shown in Fig.4, using a Voigt

line profile with essentially the same parameters. After Te adsorption, the Au_S component at 83.66eV vanishes as a result of interaction with Te. By analogy with gold oxidation, one could expect the appearance of a higher binding energy component if a gold telluride is formed, but this is not the case here. Indeed, we obtain an effect comparable to the case of Se/Au(111)[41] system and one expects a weakly-chemisorbed Te on the Au(111) surface.

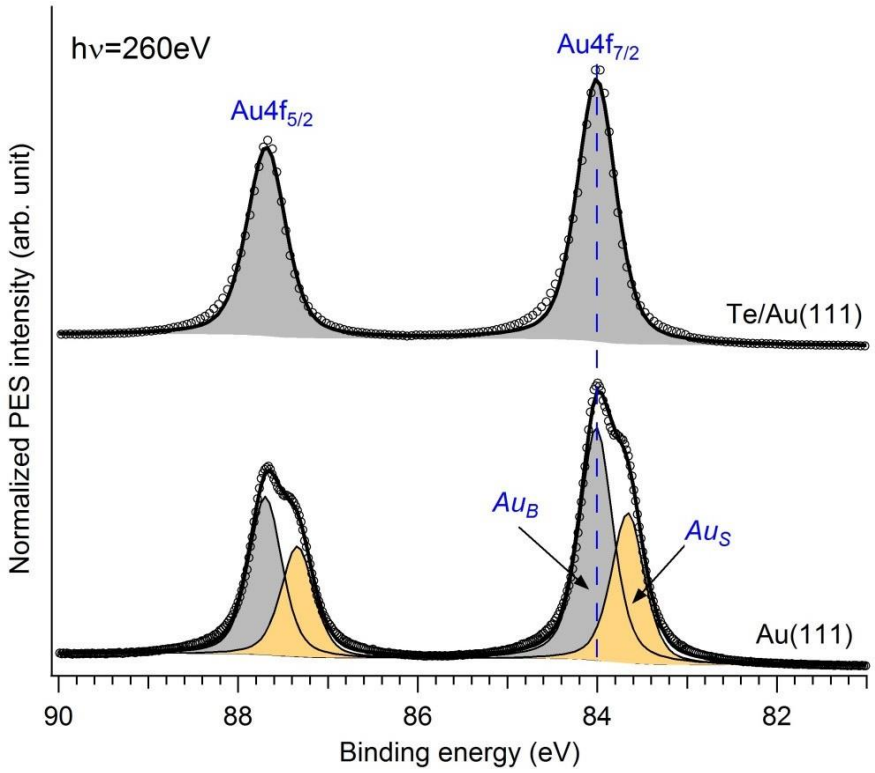

Fig.4: Core level Au4f XPS spectra recorded at normal emission before and after deposition of 0.5ML of Te on Au(111). As shown, the deconvolution of these spectra yields to two contributions for the clean substrate, Au_B stands the bulk and Au_S the surface, while only the Au_B one is present after growing Te on the surface.

The Te4d core level spectra obtained on Te covering Au(111) at thicknesses ranging from 0.25ML to a thick layer (greater than 20ML) are shown in Fig.5. Two main spectroscopic structures associated with $4d_{3/2}$ and $4d_{5/2}$ core levels are observed. For a detailed analysis, we limit ourselves to the $4d_{5/2}$ characteristics in the rest of the discussion. Starting from thick-layer of Te on Au(111), the fit using voigt-like peaks of the $4d_{5/2}$ feature indicates the presence of one contribution positioned at 40.44eV and assigned to the Te bulk. This value is consistent with the binding energy obtained on Te/Cu(111) elaborated by chemical deposition method[10]. When the Te film is much thinner around 0.5ML, the shape of the photoemission spectrum remains almost unchanged, however, the peak position of the $4d_{5/2}$ level occurs shifted to 40.1eV. The peak line-width is almost identical and is about 0.54 eV. At this thickness, the surface displays (3X3) honeycomb-like reconstruction on which self-organized adatom chains are formed, as

discussed above. Surprisingly, we observed only one chemical environment, whereas one can expect at least two contributions; one related to adatom chains and the other to the (3x3) reconstruction behind. One possible explanation of this result is that both contributions have the same binding energy. This means that the atoms from chains and those of the underlying layer have comparable interactions with the Au substrate, which are in this case significantly weak. Thus, it can be suggested that the (3x3) reconstructed layer is decoupled from the Au(111) substrate and can be described as a floating monolayer of *Tellurene-type*, since it also has a honeycomb-like structure.

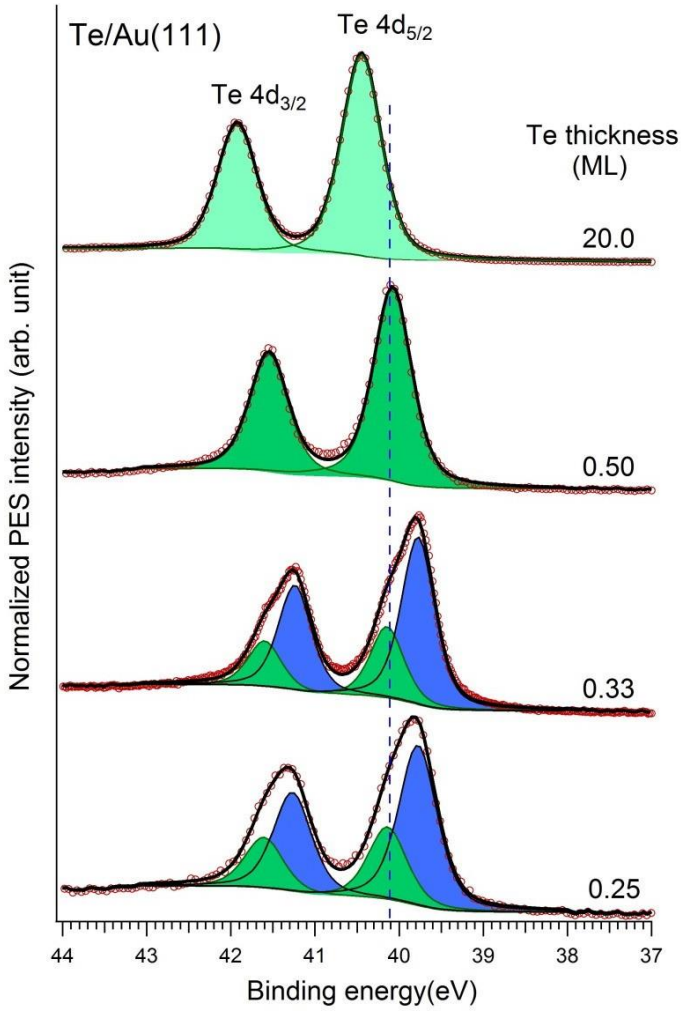

Fig.5: XPS spectra of the Te4d core levels obtained for different thicknesses of Te on Au(111). Each spectrum is deconvoluted using fit with voigt-like peaks.

When the Te thickness is about 0.33ML, the photoemission spectrum changes and exhibits features significantly asymmetric due to the presence of a shoulder at the high energy side. After a Shirley background subtraction the spectrum was deconvoluted (Fig.5) by choosing the same peak width as that used for the other thicknesses. An accurate fit required utilization of two voigt-type contributions; one is associated with the shoulder structure at binding energy of

about 40.13eV and second contribution characterized by high intensity and located at 39.77eV, as seen in Fig.5. Thus, two chemical environments of Te exist in the reconstruction shown in Fig.2d. In fact, upon decreasing the Te coverage, the Te contribution associated with (3x3) becomes weaker and new structure develops. The shape of the XPS spectrum does not change too much when the Te coverage is about 0.25ML and exhibits two spectroscopic features at the same energies as for 0.33ML. Indeed, this indicates the existence of two different chemical vacancies, one at 40.13eV corresponds to Te weakly bond to the substrate and the second at 39.77eV is supposed to be related to the Te-Au chemical bonding which suggests the presence of alloy monolayer giving rise to the ($\sqrt{3}$x$\sqrt{3}$)R30° reconstruction. Thus, the XPS data indicate a phase transition as a function on the Te coverage; the formation of Surface alloy which transforms progressively into decoupled Te monolayer. This result is consistent with the STM analysis, suggesting the existence of a tellurene-type monolayer.

The Shockley state (SS) represents a sensitive probe of the interaction strength at the deposit/metal interface and of the resulting physical processes such as charge transfer. Here, we investigated by ARPES the modification of the Au(111) Shockley state after deposition of Te film. Fig.6 shows the photoemission intensity in grey-scale $I(E_B,k_{II})$ as a function of the binding energy E_B and the in-plane component k_{II} of the wave vector along Γ--M direction of the SBZ.

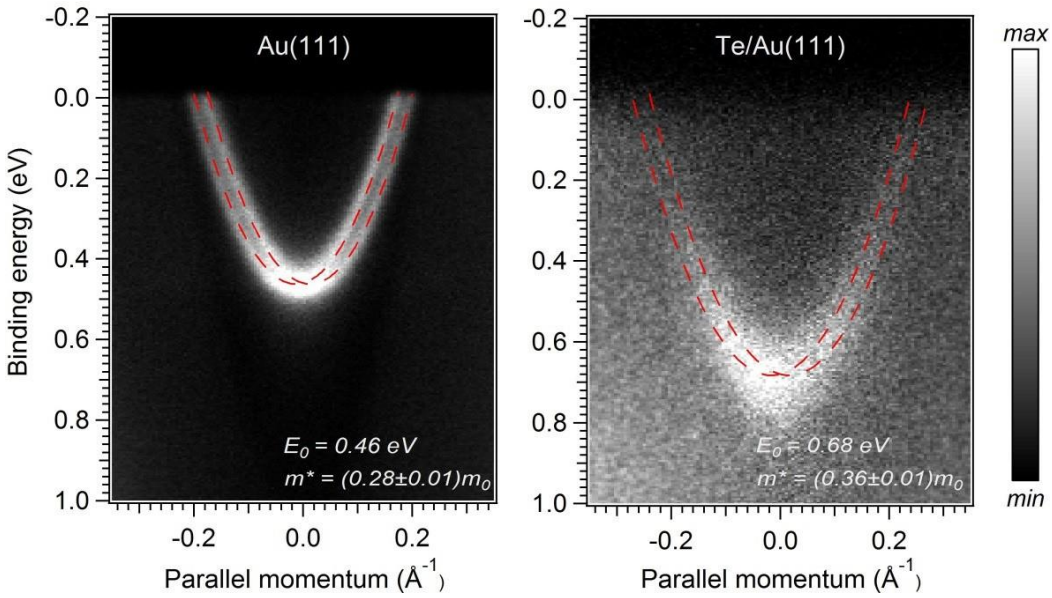

Fig.6: Shockley state bands measured by ARPES on pristine Au(111) (left panel) and on Au(111) covered by 0.33 ML of Te (right panel). The ARPES data have been recorded at normal emission along Γ-M direction and at T=100K with a photon energy of 60eV.

As seen in Fig.6, the Shockley state of pristine Au(111) corresponds to two parabolic electron dispersion shifted in the right and in the left from the Γ-point. This net offset in the *k*-direction

represents to the Rashba spin-orbit (RSO) splitting, which is well described in the literature[42,43], also for other systems[44,45].

After deposition of 0.33ML of Te, we observe a significant downward energy shift of the Shockley state band, which is attributed to an electron transfer process from the Te atoms to the Au(111) surface. Also, there is a significant change in the effective mass, whereas it is not obvious to estimate the variation in the RSO splitting due to the broadening of the peak, which is attributed to the effect of the high anisotropy of the surface reconstruction causing a loss of momentum conservation of the emitted photoelectron and hence leading to a significant decay of the Shockley state intensity and to a high background. The contribution of undesirable adsorbates such as oxygen, carbon or water is totally excluded since the XPS indicated an Au(111) surface free of such molecules. To obtain the Shockley state parameters for Te/Au(111), we used the dispersion formula of a nearly free electron behavior, in which we assumed the same RSO amplitude as for pristine Au(111). Thereby, its energy dispersion can be described within the Bychkov-Rashba (BR)[46] model as: $E_{\pm}(\vec{k}) = E_0 + \frac{h^2 k^2}{2m^*} \pm \alpha_R |k|$, where ± refers to the two spin states, α_R is the Rashba parameter, E_0 is the bottom band energy and m^* represents the effective mass. The binding energy of the bottom band lies at 0.68 eV, while its value is found to be 0.46 eV on clean Au(111). Likewise, the effective mass increases to $(0.36\pm0.01)m_0$ (m_0 denotes the free electron mass) compared to its value $(0.28\pm0.01)m_0$ on free Au(111) surface. This can be ascribed to the Te-induced significant structural and chemical change of the in-plane gradient of the surface potential, besides the presence of reconstructions which can also have an effect.

By performing scans throughout the SBZ, we were able map the overall band structure of Te/Au(111), to gain insight on the behavior of valence electrons. Fig.7 shows a wide energy scan along the ΓK and ΓM directions of the SBZ recorded on Au(111) surface covered by 0.33ML of Te. Besides the Shockley states around the Γ-point, we observe highly dispersive bands crossing the Fermi level, which correspond to the *sp*-states of the Au(111) surface. Additionally, we distinguish broad bands having a parabolic-type dispersion with negative effective mass, labeled S_1 and S_2. By analogy with a sister system $Cu_2Te/Cu(111)$, those bands can originate from the Te adsorbates inducing an Au_2Te alloy at the surface and result from strong hybridization between the Au *5d/6s* and Te *5p* orbitals. Moreover, we observe a back-folding behavior of these bands in the adjacent reduced SBZ (R-SBZ) of the $(\sqrt{3} \times \sqrt{3})R30°$ superstructure, which is a typical behavior of a 2D electron system. As seen in Fig.7, these hybridization bands are characterized by low intensity, as the photoelectrons are probably

strongly scattered by the profound corrugation of the long range moiré structure. On the other hand, along Γ-M direction, it is seen that the Shockley state band in second SBZ is back-folded due also to the effect of the moiré superstructure of the surface alloy observed by STM. This finding suggests the formation of 2D like electrons system localized at the Au_2Te surface alloy. The ARPES data reveal also a semiconductor character of the Au_2Te monolayer with a gap limit of about 0.65 eV, which in agreement with the STS measurements given in ref.[25].

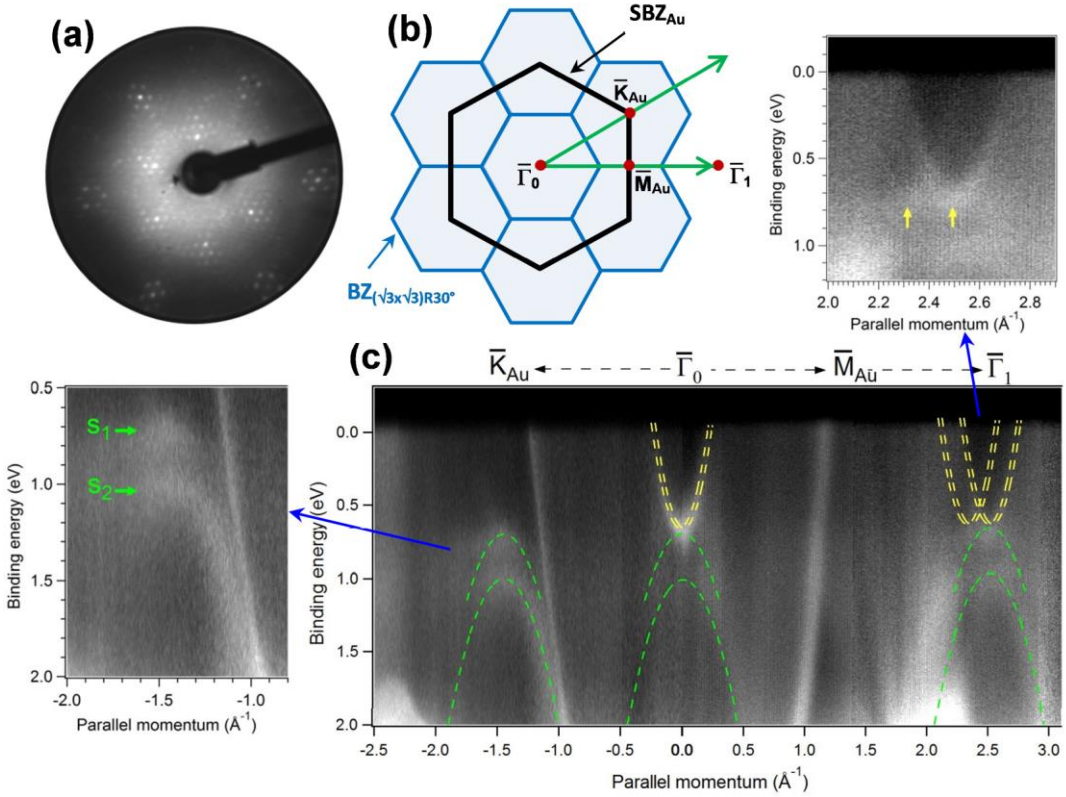

Fig.7: (a) LEED pattern and (b) the corresponding schematic of the SBZs of the (√3x√3)R30° reconstruction obtained after deposition of 0.33ML of Te on Au(111) surface. (c) ARPES mapping of band structure along K-Γ-M-Γ directions measured also on Au(111) covered by 0.33 ML of Te. The ARPES data have been recorded at T=100K with a photon energy of 60eV and the LEED pattern measured at energy of 80 eV.

By increasing the Te coverage to 0.5ML, the surface reconstruction changes radically and as discussed above the upper layer has a honeycomb-like network similar to that of graphene. The band structure also changes, as shown in Fig. 8, where we report the ARPES mapping along the ΓM direction of the SBZ. First, we observe persistence of the Shockley state band, although it appears much broadened and shifted back towards its original position of clean Au(111). This is a signature of a weakening of the interaction between the Te layer and the Au substrate, in good agreement with the XPS data. Furthermore, a new band that we label S_3 occurs at a bottom binding energy of 0.65eV and is characterized by a peculiar *invert U* shape, i.e almost

flat around the center and dispersing to high binding energy at the SBZ boundaries. After a close inspection, we found that this band lies at the Γ point of the third R-SBZ associated with the (3x3) superstructure, which is consistent with the LEED pattern displaying second order spots with high intensity compared to the other diffraction spots, as shown in Fig.8a. The absence of such band at the Γ point of the first SBZ can be attributed to a matrix element effect. The presence of such a band can be the signature of the Tellurene-like monolayer and its energy position indicates a semiconductor character of this latter.

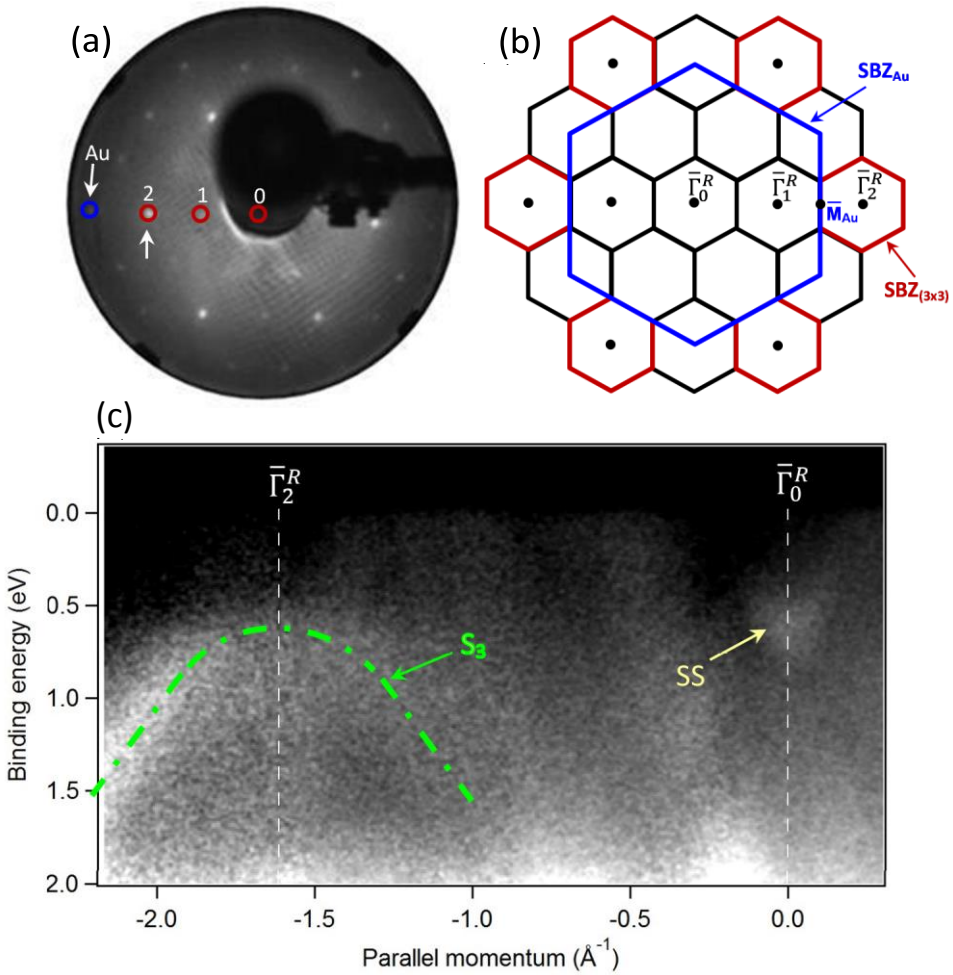

Fig.8: (a) LEED pattern obtained on Au(111) surface covered by 0.5ML of Te, showing (3x3) reconstruction and (b) the corresponding surface Brillouin zone. (c) ARPES results obtained on the same surface along the ΓM directions of the Au(111) SBZ.

4. Conclusion

We have studied here the changes in the structural and electronic properties of Au(111) surface induced after deposition of Te. At large distance, LEED and STM analyses indicated the formation of well-ordered and long-range reconstructions, however, details at the atomic scale demonstrated rich and complicated structures depending on the Te coverage. The XPS data

indicated the formation of an Au_2Te surface alloy at Te thickness below 0.33ML and a transition to a so-called tellurene monolayer with a unique chemical environment when the Te coverage reaches 0.5ML. The existence of a single Au chemical environment ruled out the possible formation of AuTe2, which is one of the scenarios discussed here. By ARPES, new dispersive bands were revealed at 0.33ML, which originate from a strong hybridization between Te and Au electronic states. These bands are strongly influenced by the surface reconstructions and undergo folding at the boundaries of the reduced surface Brillouin zone. This finding clearly highlights the presence of 2D-type electron system within the AuTe alloy layer. More interesting, the band structure changes when the tellurene-like monolayer is formed at 0.5ML and a peculiar band is observed. The ARPES data reveal the existence of a band gap and suggest a semiconductor character of the Au_2Te surface alloy and also of the tellurene monolayer.

Acknowledgments

M. B. and A. B. acknowledges for Synchrotron SOLEIL direction for supporting the project. We thank also the TEMPO beamline staff for the technical support. W. Zhang and Y. Tong are grateful to the China Scholarship Council (CSC) for the financial support (scholarship) for their Ph.D. works in France.

References

1. Wang, Q. H.; Kalantar-Zadeh, K.; Kis, A.; Coleman, J. N.; Strano, M. S.; Electronics and Optoelectronics of Two-Dimensional Transition Metal Dichalcogenides. Nature Nanotech. 2012, 7, 699-712.
2. Mark, K. F.; Lee, Ch.; Hone, J.; Shan, J.; Heinz, T. F. Atomically Thin MoS_2: A New Direct-Gap Semiconductor. Phys. Rev. Lett. 2010, 105, 136805.
3. Splendiani, A.; Sun, L.; Zhang, Y.; Li, T.; Kim, J.; Chim, Ch. –Y.; Galli, G.; Wang, F. Emerging Photoluminescence in Monolayer MoS_2. Nano Lett. 2010, 10, 1271-1276.
4. Xi, X.; Wang, Z.; Zhao, W.; Park, J.-H.; Law, K. T.; Berger, H.; Forró, L.; Shan, J.; Mark, K. F. Ising Pairing in Superconducting $NbSe_2$ Atomic Layers. Nature Phys. 2016, 12, 139-143.
5. Saito, Y.; et al. Superconductivity Protected by Spin-Valley Locking in Ion-gated MoS_2. Nature Phys. 2016, 12, 144-149.
6. Barja, S.; et al. Charge Density Wave Order in 1D Mirror Twin Boundaries of Single-Layer MoSe2. Nature Phys. 2016, 12, 751-756.
7. Qian, X.; Liu, J.; Fu, L.; Li, J. Quantum Spin Hall Effect in Two-Dimensional Transition Metal Dichalcogenides. Science 2014, 346, 1344.
8. Cao, T. et al. Valley-Selective Circular Dichroism of Monolayer Molybdenum Disulphide. Nature Commun. 2012, 3, 887.
9. Wang, G.; Robert, C.; Suslu, A.; Chen, B.; Yang, S.; Alamdari, S.; Gerber, I. C.; Amand, Th.; Marie, X.; Tongay, S.; Urbaszek, B. Spin-Orbit Enginnering in Transition Metal Dichalcogenide Alloy Monolayers, Nature Comm. 2015, 6, 10110.
10. Tong, Y.; Bouaziz, M.; Zhang, W.; Obeid, B.; Loncle, A.; Oughaddou, H.; Enriquez, H.; Chaouchi, K.; Esaulov, V.; Chen, Z.; Xiong, H.; Cheng, Y.; Bendounan, A. Evidence of New 2D Material: Cu_2Te. 2D Mater. 2020, 7, 035010.
11. Qian, K.; Gao, L.; Li, H.; Zhang, S.; Yan, J. H.; Liu, C.; Wang, J. O.; Qian, T.; Ding, H.; Zhang, Y. Y.; Lin, X.; Du, S. X.; Gao, H-J. Epitaxial Growth and Air-Stability of Monolayer Cu_2Te. Chinese Phys. B 2020, 29, 018104.

12. Wang, Y.; et al. Monolayer $PtSe_2$, a New Semiconducting Transition-Metal-Dichalcogenide, Epitaxially Grown by Direct Selenization of Pt. Nano Lett. 2015, 15, 4013-4018 (2015).
13. Tong, Y.; Bouaziz, M.; Oughaddou, H.; Enriquez, H.; Chaouchi, K.; Nicolas, F.; Kubsky, S.; Esaulov, V.; Bendounan, A.; Phase Transition and Thermal Stability of Epitaxial $PtSe_2$ Nanolayer on Pt(111). RSC Adv. 2020, 10, 30934-30943.
14. Lin, M.-K.; Villaos, R. A. B.; Hlevyack, J. A.; Chen, P.; Liu, R.-Y.; Hsu, C.-H.; Avila, J.; Mo, S.-K.; Chuang, F.-C.; Chiang, T.-C. Dimensionality-Mediated Semimetal-Semiconductor Transition in Ultrathin $PtTe_2$ Films. Phys. Rev. Lett. 2020, 124, 036402.
15. Gu, C.; Zhao, S.; Zhang, J. L.; Sun, S.; Yuan, K.; Hu, Z.; Han, C.; Ma, Z.; Wang, L.; Huo, F.; Huang, W.; Li, Z.; Chen, W. Growth of Quasi-Free-Standing Single-Layer Blue Phosphorus on Tellurium Monolayer Functionalized Au(111). ACS Nano 2017, 11, 5, 4943-4949.
16. Yang, B.; et al. Te-Doped Black Phosphorus Field-Effect Transistors, Adv. Mater. 2016, 28, 9408-9415.
17. Ootsuki, D.; et al. Effect of Pt Substitution on the Electronic Structure of $AuTe_2$. Phys. Rev. B 2014, 90, 144515.
18. Kudo, K.; Ishii, H.; Nohara, M. Composition-Induced Structural Instability and Strong-Coupling Superconductivity in $Au_{1-x}Pd_xTe_2$. Phys. Rev. B 2016, 93, 140505(R).
19. Kitagawa, S.; Kotegawa, H.; Tou, H.; Ishii, H.; Kudo, K.; Nohara, M.; Harima, H. Pressure-Induced Superconductivity in Mineral Calaverite AuTe2. J. Phys. Soc. Jpn. 2013, 82, 113704.
20. Deng, J.; Xia, B.; Ma, X.; Chen, H.; Shan, H.; Zhai, X.; Li, B.; Zhao, A.; Xu, Y.; Duan, W.; Zhang, S.-C.; Wang, B.; Hou, J. G. Epitaxial Growth of Ultraflat Stanene with Topological Band Inversion. Nature Materials 2018, 17, 1081-1086.
21. Ahmed, R.; Nakagawa, T.; Mizuno, S.; Structure Determination of Ultra-Flat Stanene on Cu(111) Using Low Energy Electron Diffraction. Surf. Sci. 2020, 691, 121498.
22. Wu, W.; Qiu, G.; Wang, Y.; Wang, R.; Ye, P. Tellurene: its Physical Properties, Scalable Nanomanufacturing, and Device Applications. Chem. Soc. Rev. 2018, 47, 7203-7212.
23. Wang, Y.; Qiu, Gang, Wang, R.; Huang, S.; Wang, Q.; Liu, Y.; Du, Y.; Goddard, W. A.; Kim, M. J.; Xu, X.; Ye, P. D.; Wu, W. Field-Effect Transistors Made from Solution-Grown Two-Dimensional Tellurene. Nature Electronics 2018, 1, 228-236.
24. Shen, C.; et al. Tellurene Photodetector with High Gain and Wide Bandwidth. ACS Nano 2020, 14, 1, 303-310.
25. Guan, J.; Huang, X.; Xu, X.; Zhang, S.; Jia, X.; Zhu, X.; Wang, W.; Guo, J. Superstructures at Te/Au(111) Interface Evolving upon Increasing Te Coverage. Surf. Sci. 2018, 669, 198-203.
26. Schouteden, K.; Debehets, J.; Muzychenko, D.; Li, Z.; Seo, J. W.; Van Haesendonck, C. Adsorption of Te Atoms on Au(111) and the Emergence of an Adatom-Induced Bound State. J. Phys.: Condens. Matter. 2017, 29, 125001.
27. Sorenson, T. A.; Varazo, K.; Suggs, D. W.; Stickney, J. L. Formation of and Phase Transitions in Electrodeposited Tellurium Atomic Layers on Au(111). Surf. Sci. 2001, 470, 197-214.
28. Nagashima, S. Growth Modes and Surface Structures of Te Overlayers Deposited on Au(111) Surfaces. Appl. Surf. Sci. 1999, 144-145, 73-77.
29. Hayden, B. E.; Nandhakumar, I. S. In-Situ STM Study of Te UPD Layers on Low Index Planes of Gold. J. Phys. Chem. B 1997, 101, 7751-7757.
30. Ikemiya, N.; Iwai, D.; Yamada, K.; Vidu, R.; Hara, S. Atomic Structures and Growth Morphologies of Electrodeposited Te Film on Au(100) and Au(111) Observed by In-Situ Atomic Force Microscopy. Surf. Sci. 1996, 369, 199-208.
31. Barth, J. V.; Brune, H.; Ertl, G.; Behm, R. J. Scanning Tunneling Microscopy Observations on the Reconstructed Au(111) surface: Atomic Structure, Long-Range Superstructure, Rotational Domains, and Surface Defects. Phys. Rev B 1990, 42, 9307.
32. Wang, Y.; Hush, N. S.; Reimers, J. R. Simulation of the Au(111)-(22x$\sqrt{3}$) Surface Reconstruction. Phys. Rev. B 2007, 75, 233416.
33. Kelly, R. E. A.; Xu, W.; Lukas, M.; Otero, R.; Mura, M.; Lee, Y.-J.; Laegsgaard, E.; Stensgaard, I.; Kantorovich, L. N.; Besenbacher, F. An Investigation into the Interactions Between Self-Assembled Adenine Molecules and a Au(111) Surface. Small 2008, 4, 1494-1500.
34. Kezilebieke, S.; Amokrane, A.; Boero, M.; Clair, S.; Abel, M.; Bucher, J.-P. Steric and Electronic Selectivity in the Synthesis of Fe-TCNB Complexes on Au(111): from Topological Confinement to Bond Formation. Nano Research 2014, 7, 888-897.

35. Maniraj, M.; Jungkenn, D.; Shi, W.; Emmerich, S.; Lyu, L.; Kollamana, J.; Wie, Z.; Yan, B.; Cinchetti, M.; Mathias, S.; Stadtmüller, B.; Aeschlimann, M. Structure and Electronic Properties of the ($\sqrt{3}$x$\sqrt{3}$)R30° $SnAu_2$/Au(111) Surface. Phys. Rev. B 2018, 98, 205419.
36. Shah, J.; Sohail, H. M.; Uhrberg, R. I. G.; Wang, W. Two-Dimensional Binary Honeycomb Layer Formed by Ag and Te on Ag(111). J. Phys; Chem. Lett. 2020, 11, 5, 1609-1613.
37. Ast, Ch. R.; Henk, J.; Ernst, A.; Moreschini, L.; Falub, M. C.; Pacilé, D.; Bruno, P.; Kern, K.; Grioni, M. Giant Spin Splitting through Surface Alloying. *Phys. Rev. Lett.* 2007, 98, 186807.
38. Moreschini, L.; Bendounan, A.; Bentmann, H.; Assig, M.; Kern, K.; Reinert, F.; Henk, J.; Ast, C. R.; Grioni, M. Influence of the Substrate on the Spin-Orbit Splitting in Surface Alloys on (111) Noble Metal Surfaces. *Phys. Rev. B* 2009, 80, 035438.
39. Moreschini, L.; Bendounan, A.; Gierz, I.; Ast, C. R.; Mirhosseini, H.; Höchst, H.; Kern, K.; Henk, J.; Ernst, A.; Ostanin, S.; Reinert, F.; Grioni, M. Assessing the Atomic Contribution to the Rashba Spin-Orbit Splitting in Surface Alloys: Sb/Ag(111). Phys. Rev. B 2009, 79, 075424.
40. Yeh, J. J.; Lindau, I. Atomic Subshell Photoionization Cross Sections and Asymmetry Parameters: $1 \leq Z \leq 103$. Atomic Data and Nuclear Data Tables 1985, 32, 1-155.
41. Jia, J.; Bendounan, A.; Kotresh, H. M. N.; Chaouchi, K.; Sirotti, F.; Sampath, S.; Esaulov, V. A. Selenium Adsorption on Au(111) and Ag(111) Surfaces: Adsorbed Selenium and Selenide Films. J. Phys. Chem. C 2013, 117, 9835-9842.
42. Hoesch, M.; Muntwiler, M.; Petrov, V. N.; Hengsberger, M.; Patthey, L.; Shi, M.; Falub, M.; Greber, T.; Osterwalder, J. Spin Structure of the Shockley Surface State on Au(111). Phys. Rev. B 2004, 69, 241401(R).
43. Henk, J.; Ernst, A.; Bruno, P. Spin Polarization of the L-Gap Surface States on Au(111). Phys. Rev. B 2003, 68, 165416.
44. Forster, F.; Bendounan, A.; Reinert, F.; Grigoryan, V. G.; Springborg, M. The Shockley-type Surface State on Ar Covered Au(111): High Resolution Photoemission Results and the Description by Slab-Layer DFT Calculations. Surf. Sci. 2007, 601, 5595-5604.
45. Bendounan, A.; Aït-Ouazzou, S. Role of the Shockley State in Doping of Organic Molecule Monolayer. J. Phys. Chem. C 2016, 120, 11456-11464.
46. Bychkov, Y. A.; Rashba, É. I. Properties of a 2D Electron Gas with Lifted Spectral Degeneracy. JETP Lett. 1984, 39, 78-81.